Electronic Supplementary Information

Ultrasensitive Detection of Thrombin Using Surface Plasmon Resonance and Quartz Crystal Microbalance Sensors by Aptamer-Based Rolling Circle Amplification and Nanoparticle Signal Enhancement

Peng He[1], Lijun Liu[1], Wenping Qiao[1], Shusheng Zhang[2]*

[1]*Key Laboratory of Sensor Analysis of Tumor Marker, Ministry of Education, College of Chemistry and Molecular Engineering, Qingdao University of Science and Technology, Qingdao 266042, P.R.China.*

[2]*College of Chemistry and Chemical Engineering, Linyi University, Linyi 276005, P. R. China. Fax : (+86) 532-84022750; Tel: (+86) 532-84022750; E-mail : shushzhang@126.com*

Experimental Section

Reagents. All oligonucleotides used in the present study were synthesized and purified by Shanghai Sangon Biological Engineering Technology & Services Co., Ltd.(China). Their sequences are listed in Table S1. Phi29 DNA Polymerase, 10 $U\mu L^{-1}$ and T4 DNA Ligase, 5 $U\mu L^{-1}$ were purchased from Thermo Fisher Scientific (China) Co., Ltd. The mixture of four dNTPs (2.5 mM for each component) was purchased from SBS Genetech Co .,Ltd. Hydrogen tetrachloroaurate(III) tetrhydrate ($HAuCl_4 \bullet 4H_2O$) were ordered from Sigma-Aldrich,the trisodium citrate was ordered from Tianjin Bodi chemical industry Co., Ltd.. Other chemicals employed were of analytical reagent grade and were used without further purification. Doubly distilled water was used throughout the experiments. The gold chips used for SPR detection were purchased from BioNavis Ltd (Finland). All reagents were analytical grade and used without further purification.

Table S1. DNA sequences used in this work.

Name	Sequences	Discription
S1	5'-SH-$(CH_2)_6$-TTTTTTTTGCAGTCACCCTTTTAGTCCGTG GTA GGG CAG GTT GGG GTG ACTGCTT-3'	Hairpin aptamer probe (capture probe)
S2	5'-GGTTGGTGTGGTTGGTTTTTTTTTCGAGTCAGAGGT GTGGA GTC -3'	Aptamer-primer complex
S3	5'-PO_4-CTCTGACTCGTCGTTCGCCGTTCTAGCAAAATC GTTCGCCGTTCTAGCGACTCCACAC-3'	Padlock probe
S4	5'-SH- $(CH_2)_6$-T TTT T TC GTT CGC CGT TCT AGC-3'	Complementary with RCA product
S5	5'-SH-$(CH_2)_6$-TTT TTTCGAGGTT TTT -3'	Noncomplementary DNA as bio-bar-codes to avoid cross -reaction

Apparatus. SPR detection was performed on a SPRNavi200 (BioNavis, Finland), QCM detection was performed on a Q-sense instrument (Q-Sense E1, Vastra Frolunda, Sweden). UV/Vis absorption spectra were obtained with a Cary 50 Series Spectrophotometer (Varian, Australia). Atomic Force Microscope (AFM) image was taken with a Being Nano-Instruments CSPM-4000 (Benyuan, China). Transmission electron microscopy (TEM) imaging was taken with JEM-2000EX/ASID2 instrument (Hitachi, Japan). Scanning electron microscopy (SEM) imaging was performed by a JEOL JSM-6700F instrument (Tokoy, Japan).

Preparation of Au NPs and Au NPs bio-barcode probe

Gold nanoparticles (AuNPs) were synthesized following the previously reported method by reduction of tetrachloroauric acid ($HAuCl_4$) with sodium citrate.[1] The prepared gold nanoparticles were stored in brown glass bottles at 4 ℃ and characterized by TEM (Figure S1). The Au NP bio-barcode probe was obtained by capping the DNA S4 and DNA S5 on the surface of AuNPs. The process of Au NP bio-barcode probe according a literature[2,3] was enforced as follows: the 10^{-6} M DNA S5 and 10^{-7} M DNA S4 with different molar ratios (5:1, 10:1, 20:1, 30:1, 40:1, 50:1) were activated with 2.0 μL of 10 mM TCEP for 1 h, and then added to 1 mL of freshly prepared gold nanoparticles with gentle shaking overnight. Over this course, the DNA -AuNP conjugates were aged in salts (0.1 M NaCl, 10 mM acetate buffer) for another 24 h. The additional reagents were removed by centrifuging at 10000 rpm for 30 min . The red precipitate was washed and centrifuged repeatly for three times. The resulting Au NPs bio-barcode probes were dispersed into a PBS buffer solution (0.01 mM, pH 7.4) and stored at 4 ℃ for further use. The successful immobilization of DNA on the AuNP surface could be observed from the UV-vis absorbance difference between the AuNPs solution before immobilization and the DNA-AuNPs solution after immobilization. A surface coverage density was determined by a previously reported method. [2,4,5]

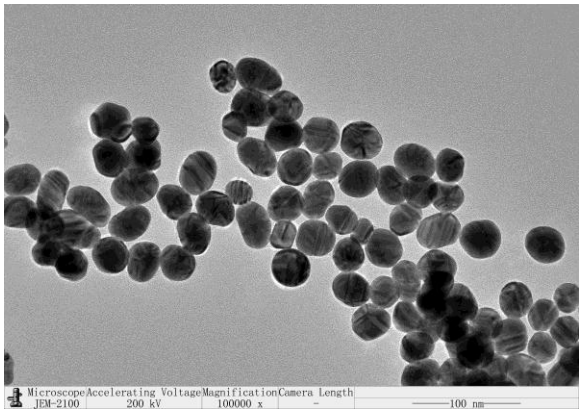

Figure S1. TEM images of AuNPs

Preparation of hairpin aptamer probe-modified Substrate

Before the modification of hairpin aptamer probe, the gold chip was immersed in a boiling solution (30% H_2O_2, 28% ammonia, and double distilled water in a volume ratio of 1:1:5) for 10 min. Then the cleaned chip was rinsed thoroughly with double distilled water, and dried by nitrogen gas prior to use. Meanwhile, the poly(dimethylsiloxane) PDMS film with the empty hole was cleaned in the ethyl

alcohol by the ultrasonic cleaner for a three minutes then rinsed by pure water and dried by nitrogen. After the PDMS film was immobilized onto the chip, 30μL of 10^{-6} M DNA S1 was added to the holes of the PDMS film to self-assemble on the surface for 16h. Subsequently, the 6-mercapto-1-hexanol (MCH) was added to the holes to block the nonspecific binding sites for 2h. Finally, the gold chips were successively rinsed with D.I. water and PBS solution to remove free and excess DNA.

Rolling Circle Amplification (RCA) Reaction

20 μL of 10^{-6} M aptamer-primer probe and 20 μL of 10^{-6} M padlock probe were mixed in a centrifugal tube. Then, 0.5 μL of T4 DNA ligase (5.0 U/μL) and 2.5 μL of T4 DNA ligase buffer were added in the DNA solution. This complex were incubated at 37 ℃ with gentle shake for 30 min. Subsequently, the RCA reaction was carried out with the addition of 10 μL 10 mM dNTPs, 4 μL 10 U/μL Phi29 DNA polymerase at 37 ℃ for 90 min. After RCA reaction, the solution was immerged in the thermostatic waterbath at 75 ℃ for 15 minutes to devitalize the enzymes.

SPR Measurement

The SPR measurements were conducted using the SPRNavi200 (BioNavis, The Finland), a double-channel and prism coupling-based instrument. A gold-coated glass disk mounted on a prism through a thin layer of index-matching oil form the base of a two-channel cuvette. Different samples can be added into the two independent channels. In a kinetic measurement mode, molecular adsorption on gold-coated glass disks is followed by monitoring SPR angle (θ) or angle shifts ($\Delta\theta$) over time.

QCM-D Measurement

The QCM-D measurements were conducted using a Q-sense instrument (Q-Sense E1, Vastra Frolunda, Sweden). This instrument allows for a simultaneous measurement of resonance frequency change (Δf) and energy dissipation change (ΔD) by periodically switching off the driving power of the oscillation of the sensor crystal and recording the decay of the damped oscillation. The 5-MHz, AT-cut quartz crystals (Q-Sense E1) were used as the reaction carriers.

Online Assay Procedures

The modified gold chip was washed by flowing PBS buffer (50 μL min^{-1} flow rate) until the baseline was constant. Then, various concentration of thrombin was injected and bound to the immobilized capture probe at 10 μL min^{-1} flow rate. Weakly bound and unbound thrombin was removed by the buffer

at 100 μL min^{-1} flow rate. After the stable baseline was obtained, the RCA products were injected allowing them to bind to the immobilized thrombin. Subsequently, the bio-bar-code AuNPs were injected and hybridized with the RCA products. Finally, the substrate was washed with buffer and the difference in the response singnal was computed by taking the difference between the initial and final buffer signals. After each measurement, the surface was regenerated by the injection of 1 M HCl.

Characterization of Au NPs bio-barcode probe

The prepared Au NPs bio-barcode probes were characterized by UV-visible spectra. As shown in Figure S2, Curve a, b respectively exhibited the characteristic absorbance of DNA S4, S5 at ~260 nm. Curve c exhibited the characteristic absorbance of gold nanoparticles (AuNPs) at ~530 nm. Curve d exhibited both the characteristic absorbance of DNA and the characteristic absorbance of AuNPs, which indicated that the AuNPs were success fully labeled with DNA. The average coverage of per Au nanoparticle was calculated (~470 DNA molecules/nanoparticle), which was comparable to the surface coverage of the oligonucleotide immobilized on the AuNPs reported by Mirkin et al.[2,3]

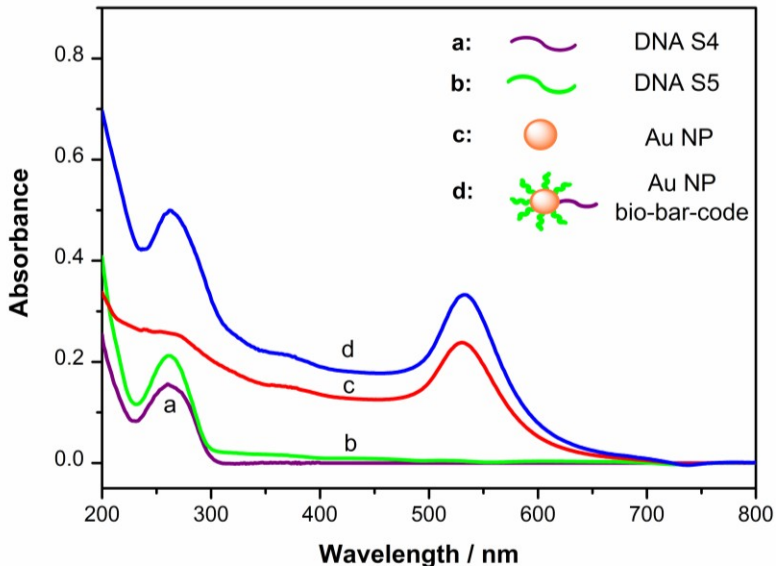

Figure S2. UV spectra of DNA S4 (a), DNA S5 (b), AuNPs (c), and Au NPs bio-barcode probe (d).

Optimization of Aptasensor Fabrication and Assay Parameters

Optimization of the aptamer pairs combination for the aptasensor. Two aptamers (15- and 29-mer) have been identified to bind with different sites of thrombin. The 29-mer aptamer (Apt29) binds to the heparin-binding site (Kd ≈ 0.5 nM), and the 15-mer aptamer (Apt15) recognizes the fibrinogen-binding site (Kd ≈ 100 nM).[6,7] Considering that two binding sites are spatially separated and localized at

opposite sides of the thrombin molecule,[8] both Apt29 and Apt15 could be used as both detection probe (conjugated with Au-NP) and capture probe (immobilized on the substrate). To obtain the best sensitivity, four aptamer pairs [Apt29 (capture probe) Apt29 (detection probe), Apt15 (capture probe) Apt15 (detection probe), Apt15 (capture probe) Apt29 (detection probe), and Apt29 (capture probe) Apt15 (detection probe)] were used to prepare aptasensors. As shown in Figure S3, the best response was obtained by using the Apt29 (capture probe) Apt15 (detection probe) pair. This is due to the fact that Apt29 has a greater affinity for α-thrombin and a more stable binding structure than Apt15.[9,10] Therefore, an Apt29 (capture probe) Apt15 (detection probe) pair was used throughout the experiments.

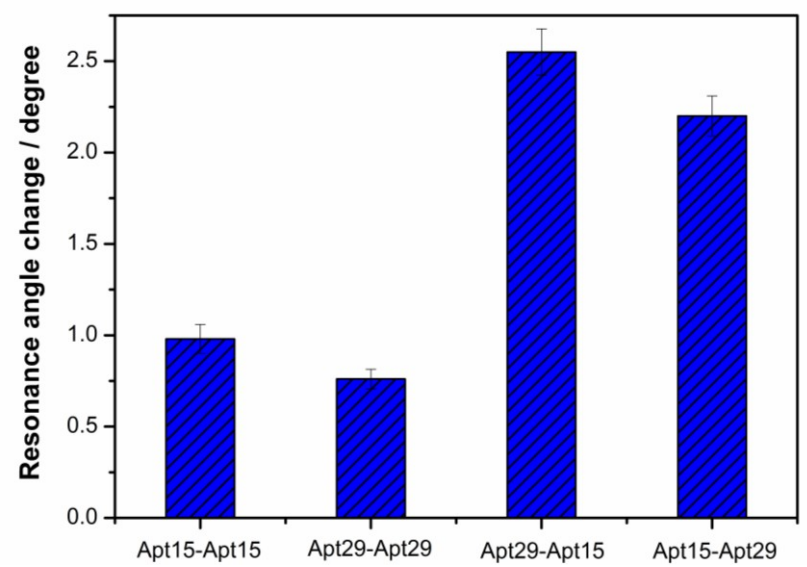

Figure S3. Responses of different aptamer pair-based aptasensors. The concentration of thrombin is 1.0×10^{-14} M.

Optimization of the detection formats. To investigate the level of the SPR signal amplification provided by the RCA-AuNPs, both online-sandwich and direct complex detection formats were evaluated for detection of thrombin. The signal is taken as a difference between the initial and final buffer injection for the calculations of signal enhancement. As illustrated in Figure S4, the dramatic signal amplification could be observed by both cases compared to the direct detection of the thrombin only. Whereas the larger amplified signal was obtained through the sandwich detection assay (Figure S4A). It is due to the increased detection specificity as demonstrated by the control curves (Figure S4A, a) and the steric hindrance from the direct injection of complex (Figure S4B, b). Therefore, the online -sandwich detection format was used throughout the experiments.

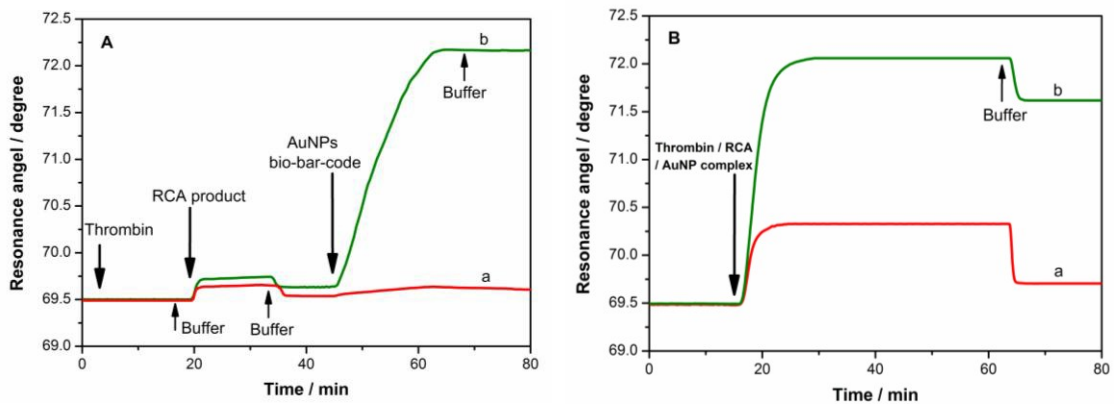

Figure S4. Responses of the sandwich detection format (A) and direct complex detection format (B): the control curves (a), and the target curves (b). The concentration of thrombin is 1.0×10^{-14} M.

Optimization of the capture substrat. To reduce the nonspecific adsorption, three different capture substrats was performed. The signal-to-background ratio was used to evaluate the assay performance. As shown in Figure S5, the highest signal-to-background ratio was observed for substrat c containing hairpin aptamer probe and MCH. The background signals observed from the reagent blank (Figure S5b) could be due to interactions between the two aptamers (Apt15 and Apt29). The two aptamers could form intermolecular G-quartet structures,[6,11,12] because of their G-rich sequences. Thus, the MCH and the hairpin structure of capture probe could be used to effectively reduce the nonspecific adsorption. The substrat c was chosed for the experiments.

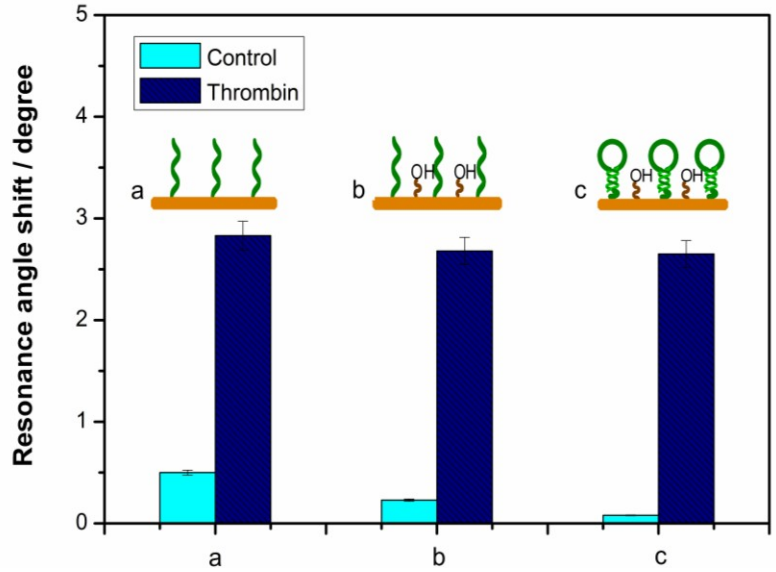

Figure S5. Optimization of the capture substrat. The thrombin in the control groups was absent, but all the other compositions and reaction steps were the same as in the detection of thrombin sample. The concentration of thrombin is 1.0×10^{-14} M. The error bars are standard deviations of three repetitive measurements.

Optimization of the concentration of the hairpin aptamer probe immobilized on the gold chip. The

hairpin aptamer probe immobilized on the gold film surface was used as the capture probe. The high concentration of hairpin structured probes might increase steric hindrance for the target binding, leading to a low signal gain.[13] On the other hand, low concentration could not bind sufficient target. Figure S6 showed the variance of SPR singnal with the concentration of capture probe. In the presence of 1.0×10^{-14} M thrombin, the SPR signal increased with the increase of probe concentration from 5.0×10^{-8} M to 1.0×10^{-6} M, reached a maximum value and then decreased monotonically beyond the concentration of 1.0×10^{-6} M. Therefore, the concentration hairpin probes of 1.0×10^{-6} M was employed in the following work.

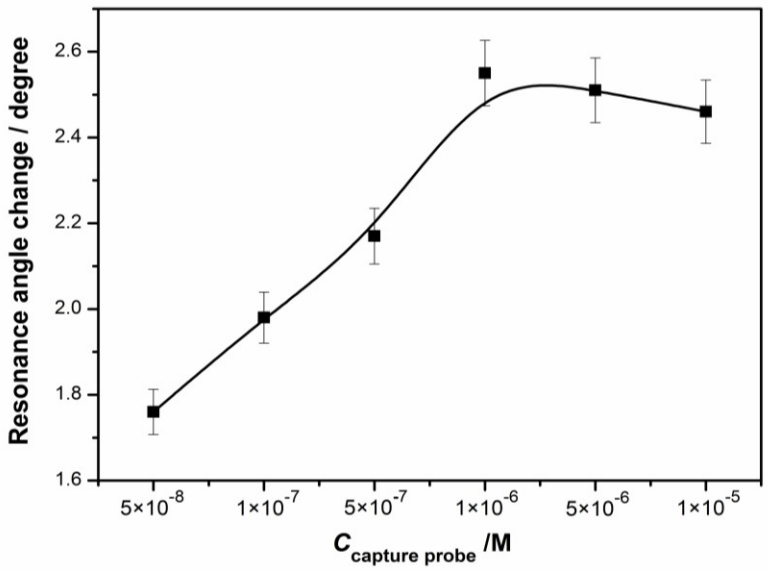

Figure S6. Effect of the concentration of the capture probe on the SPR signal.

Optimization of the size of AuNPs. To improve the sensitivity of SPR quantification of thrombin, the size of the AuNPs was optimized. In this work, Au NPs with average diameters of 12, 16, 25, 41.5, 60, and 71.5 nm, respectively, were selected. As shown in Figure S7, the SPR signal increased with the increase of AuNPs size from 12 to 41.5 nm, and reached a maximum at 41.5 nm. These results demonstrated that the oligonucleotide amount decreased with increasing AuNPs size,[3] but the large gold particles were easy to aggregate, and might increase the steric hindrance. Thus the size of 41.5 nm (see Figure S1) was selected for the subsequent assays.

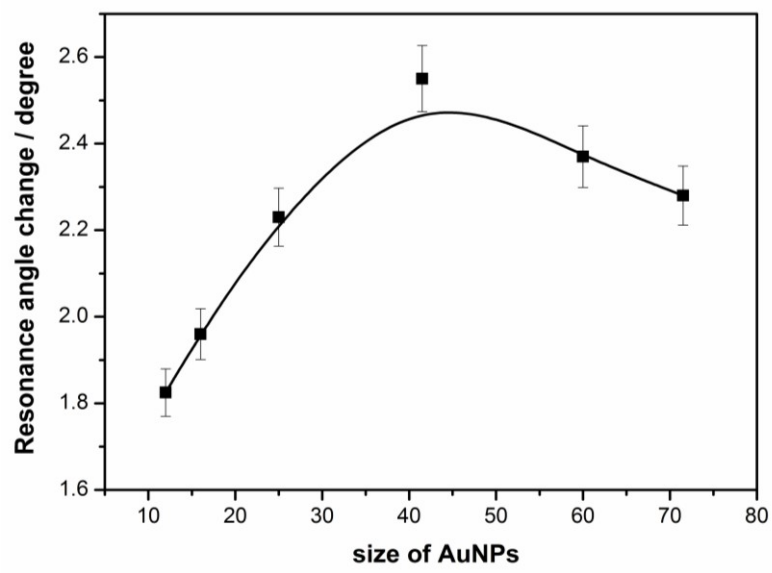

Figure S7. SPR signals for different size of AuNPs. The concentration of DNA is 1.0×10^{-14} M.

Optimization of the proportion of the bio-barcode probe immobilized on the AuNPs. The AuNPs were functionalized with DNA S4 complementary to the RCA product and DNA S5 as bio-barcodes to efficiently avoid cross-reaction. The resonance angle changes is also influenced by the proportion of the DNA S5 and the DNA S4 immobilized on the Au NPs. To improve the sensitivity of SPR quantification of thrombin, the proportion of the DNA S5 and the DNA S4 was optimized. Figure S8 shows the variance of resonance angle changes with the proportion of the DNA S5 and the DNA S4. It was obviously that signal increased upon raising the proportion from 5:1 to 20:1, and reached the maximum at 20:1. Thus the ratio of 20:1 was selected for the subsequent assays.

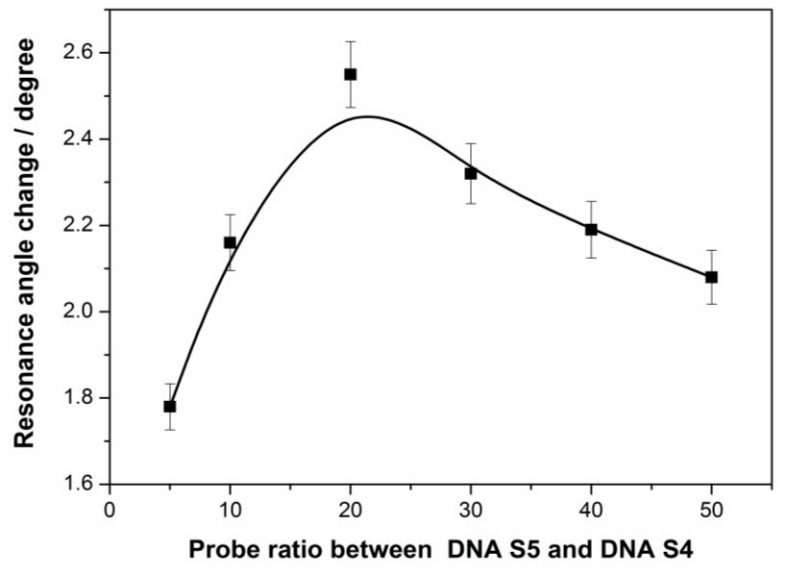

Figure S8. Resonance angle changes for different ratio of DNA S5 to DNA S4. The concentration of thrombin is 1.0×10^{-14} M.

Optimization of the amount of Phi29 DNA Polymerase. To investigate the influence of the amount of Phi29 DNA Polymerase used in the experiment of thrombin detection, the resonance angle changes produced by 1.0×10^{-14} M target thrombin were measured by using various amounts of polymerase. As shown in Figure S9, when the concentration of polymerase increased from 0.1 to 0.4 U μL^{-1}, the resonance angle changes increased gradually. After that, the resonance angle changes tended to the platform. Therefore, 0.4 U μL^{-1} of polymerase was considered to be the optimum amount used in the amplification reaction.

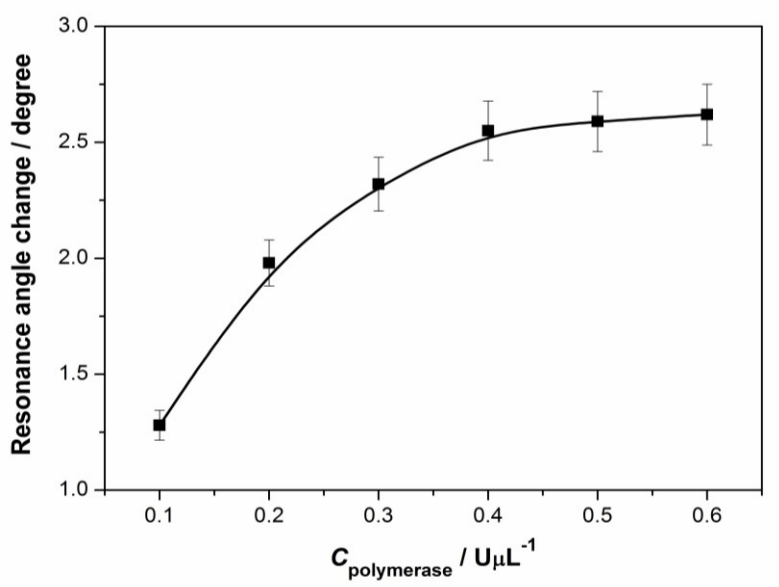

Figure S9. Influence of the amount of polymerase on the resonance angle changes responding to 1.0×10^{-14} M target thrombin.

Optimization of the temperature. The amplification temperature had a crucial effect on the reactivity of enzyme and the DNA hybridization efficiency. Figure S10 showed the influence of the temperature on the resonance angle changes produced by 1.0×10^{-14} M target thrombin. As it could be seen, a maximal resonance angle changes was obtained when the reaction temperature of the system was at 37 ℃. So we employed 37 ℃ as the optimal experimental temperature, which was consistent with the fact that enzymatic reactions are usually operated at 37 ℃ by virtue of the best bioactivity of enzymes.

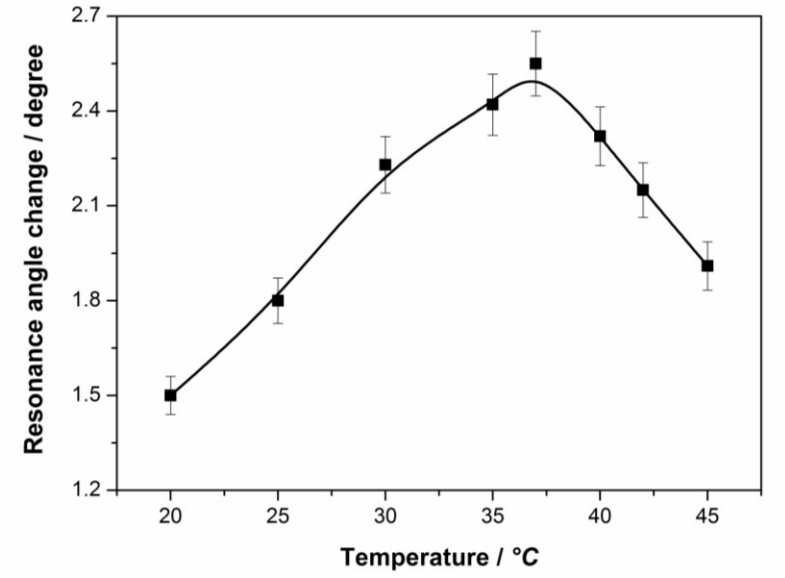

Figure S10. Influence of reaction temperature on the resonance angle changes responding to 1.0×10^{-14} M target thrombin.

Optimization of the time of RCA reaction. As shown in Figure S11, the resonance angle changes increased as the reaction time was prolonged and reached the maximum value after 90 min. Therefore, 90 min was chosen as the optimal reaction time for RCA.

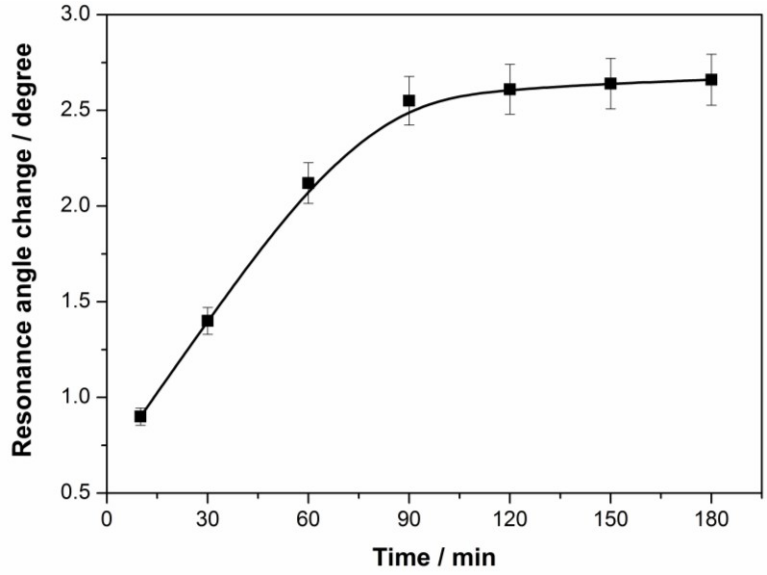

Figure S11. Influence of the RCA reaction time on the resonance angle changes responding to 1.0×10^{-14} M target thrombin.

Regeneration of the Sensor Chip

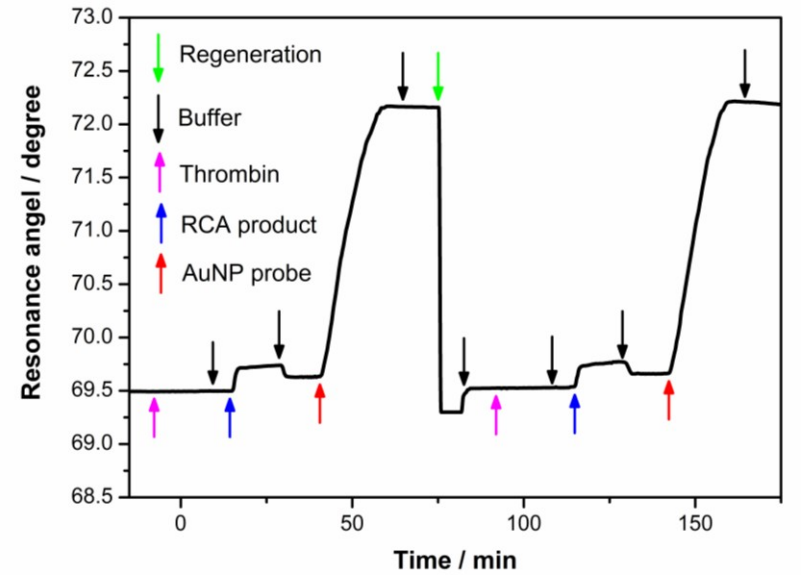

Figure S12. SPR angle-time curves showing two repeated cycles for the injections of 1.0×10^{-14} M target thrombin, RCA, AuNPs, buffer into an SPR channel covered and the regeneration of the sensor surface using 1 M HCl.

Specificity of Thrombin Detection by QCM

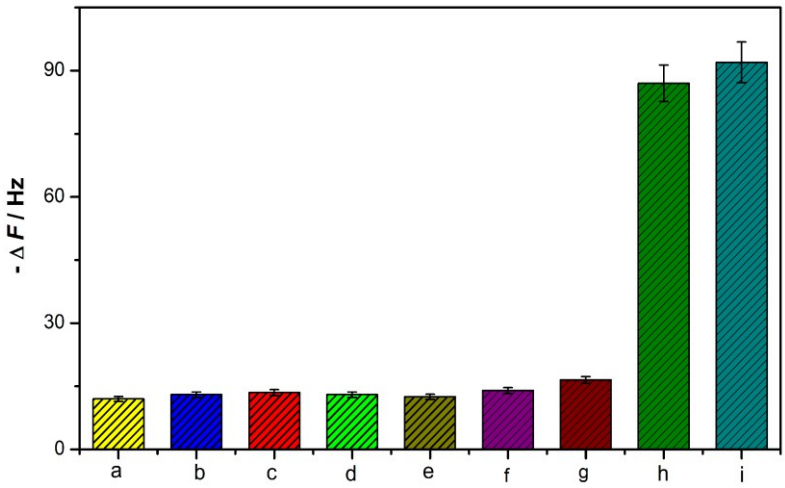

Figure S13. The frequency responses to (a) buffer, (b) AFP, (c) BSA, (d) P53, (e) lysozyme, (f) IgG, (g) human serum samples, (h) thrombin in buffer, (i) thrombin spiked in human serum. The concentration of thrombin: 100 aM, and others: 1 pM. The error bars are standard deviations of three repetitive measurements.

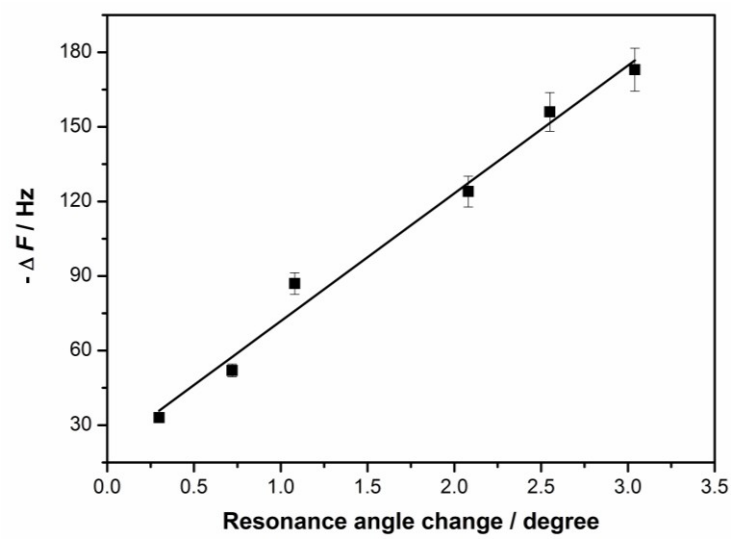

Figure S14. Comparison of the SPR and QCM results for detection of thrombin. The error bars are standard deviations of three repetitive measurements.

Table S2. Comparison of different methods for thrombin detection.

Assay	Indicator or amplification	Detection limit	ref
surface plasmon resonance imaging (SPRI)	enzyme horseradish peroxidase	500 fM	14
colorimetric detection	cyclic enzymatic signal amplification	50 pM	15
electrochemical detection	3,4,9,10-Perylenetetracarboxylic Acid/Hemin nanocomposites	1 pM	16
electrochemiluminescence detection	DNA cycle amplification	1 fM	17
electrochemical detection	molecularly grafted aptamer on graphene	0.45 fM	18
surface plasmon resonance	quasi-spherical gold nanoparticle	1 aM	19
electrochemiluminescence detection	gold nanoparticles	26 aM	20
electrochemical detection	PCR amplification	5.4 fM	21
colorimetric detection	nicking enzyme assisted signal amplification and DNAzyme amplification	1.5 pM	22
chemiluminescent detection	unmodified gold nanoparticles	26 fM	23
electrochemiluminescence detection	magnetic Fe3O4@CdSe composite quantum dot (QD)	120 fM	24
electrochemical detection	enzyme-precipitate-coating-linked aptamer	13.5 pM	25
electrochemical detection	post-labeling strategy based on dye-induced peeling of the aptamer off SWNTs	3 pM	26
electrochemical detection	network-like thiocyanuric acid / gold nanoparticles	7.82 aM	27
surface enhanced Raman scattering	target-triggering cascade multiple cycle amplification and gold nanoparticles	86 fM	28

microfluidic scanning	aptamer-functionalized microgel particles	4 pM	29
electrochemical detection	gold nanoparticles doped conducting polymer nanorod	0.14 pM	30
surface plasmon resonance	aptamer / thrombin / aptamer-AuNPs sandwich	0.1 nM	31
electrochemical detection	chitosan–Au nanocomposites	5.5 fM	32
fluorescence detection	nicking enzyme amplification	2 pM	33
surface plasmon resonance	AuNP-tagged RCA	0.78 aM	this work
quartz crystal microbalance	AuNP-tagged RCA	0.8 aM	this work

Practical Determination of Thrombin in serum samples

Recovery ratio of the assay in the blood samples by SPR[a]

Table S3 Recovery ratio of the assay in the blood samples

	Thrombin added	content	Thrombin detected	content	Recovery (%)	RSD (%)
1	5×10^{-18} M		4.82×10^{-18} M		96.4%	5.3
2	1×10^{-17} M		1.03×10^{-17} M		103%	4.8
3	5×10^{-17} M		4.78×10^{-17} M		95.6%	6.2

a Each sample was repeated for three times and averaged to obtain the recovery and RSD values.

Recovery ratio of the assay in the blood samples by QCM[b]

Table S4 Recovery ratio of the assay in the blood samples

	Thrombin added	content	Thrombin detected	content	Recovery (%)	RSD (%)
1	5×10^{-18} M		4.88×10^{-18} M		97.6%	5.6
2	1×10^{-17} M		1.04×10^{-17} M		104%	7.4
3	5×10^{-17} M		5.26×10^{-17} M		105.2%	6.1

b Each sample was repeated for three times and averaged to obtain the recovery and RSD values.

Table S5. The surface coverage of the Au nanoparticles[c]

	Thrombin concentration	Frequency shifts (ΔF)	Surface coverage (Δm)
	M	Hz	μg cm^{-2}
1	1×10^{-13}	165.89	2.93
2	1×10^{-15}	121.43	2.15
3	1×10^{-17}	54.31	0.96

c The surface coverage of the Au nanoparticles from QCM-D was calculated using the Sauerbrey equation.[34]

Reference

[1] G. Frens, *Nature Physical Science*, 1973, **241**, 20.

[2] T. A. Taton, C. A. Mirkin, R. L. Letsinger, *Science*, 2000**,** **289**, 1757.

[3] S. J. Hurst, A. K. R. Lytton-Jean, C. A. Mirkin, *Anal. Chem.* 2006, **78**, 8313.

[4] S. Zhang, H. Zhong, C. Ding, *Anal. Chem.*, 2008, **80**, 7206.

[5] Y. Wang, B. Liu, *Anal. Chem.,* 2007, **79**, 7214.

[6] L. C. Bock, L. C. Griffin, J. A. Latham, E. H. Vermaas, J. J. Toole, *Nature*, 1992, **355**, 564.

[7] J. Li, X. Zhong, H. Zhang, X. C. Le, and J. Zhu, *Anal. Chem.*, 2012, **84**, 5170.

[8] S. Poniková, K. Tlučková, M. Antalík, V. Víglaský, T. Hianik, *Biophys. Chem.*, 2011, **155**, 29.

[9] D. M. Tasset, M. F. Kubik, W. J. Steiner, *Mol. Biol.*, 1997, **272**, 688.

[10] Y. H. Lao, K. Peck, L. C. Chen, *Anal. Chem.*, 2009, **81**, 1747.

[11] Q. Zhao, X. Lu, C. Yuan, X. Li, and X. C. Le, *Anal. Chem.*, 2009, **81**, 7484.

[12] J. T. Davis, *Angew. Chem., Int. Ed.*, 2004, **43**, 668.

[13] Y. Cao, S. Zhu, J. Yu, X. Zhu,Y. Yin, G. Li, *Anal. Chem.* 2012, **84**, 4314.

[14] Y. Li, H. J. Lee, and R. M. Corn, *Anal. Chem.*, 2007, **79**, 1082.

[15] J. Li, H. Fu, L. Wu, A. Zheng, G. Chen, and H. Yang, *Anal. Chem.*, 2012, **84**, 5309.

[16] Y. Yuan, R. Yuan, Y. Chai, Y. Zhuo, X. Gan, and L. Bai, *Chem.-Euro. J.*, 2012, **18**, 14186.

[17] Y. Guo, X. Jia and S. Zhang , *Chem. Commun.*, 2011, **47**, 725.

[18] Y. Wang, Y. Xiao, X. Ma, N. Li and X. Yang, *Chem. Commun.*, 2012, **48**, 738.

[19] M. J. Kwon, J. Lee, A. W. Wark, and H. J. Lee, *Anal. Chem.*, 2012, **84**, 1702.

[20] J. Wang, Y. Shan, W. Zhao, J. Xu, and H. Chen, *Anal. Chem.*, 2011, **83**, 4004.

[21] Y. Xiang, M. Xie, R. Bash, J. J. L. Chen, and J. Wang, *Angew. Chem. Int. Ed.*, 2007, **46**, 9054.

[22] Y. Huang, J. Chen, S. Zhao, M. Shi, Z. Chen, and H. Liang, *Anal. Chem.*, 2013, **85**, 4423.

[23] Y. Qi, B. Li, *Chem.-Euro. J.*, 2011, **17**, 1642.

[24] G. Jie and J. Yuan, *Anal. Chem.*, 2012, **84**, 2811.

[25] H. J. Lee, B. C. Kim, M. K. Oh and J. Kim, *Chem. Commun.*, 2012, **48**, 5971.

[26] Y. Fu, T. Wang, L. Bu, Q. Xie, P. Li, J. Chen and S. Yao, *Chem. Commun.*, 2011, **47**, 2637.

[27] J. Zheng, W. Feng, L. Lin, F. Zhang, G. Cheng, P. He, Y. Fang, *Biosens. Bioelectron.*, 2007, **23**, 341.

[28] P. He, Y. Zhang, L. Liu, W. Qiao and S. Zhang, *Chem.-Euro. J.*, 2013, **19**, 7452.

[29] R. L. Srinivas, S. C. Chapin, and P. S. Doyle, *Anal. Chem.*, 2011, **83**, 9138.

[30] M. . Rahman, J. I. Son, M. S. Won, and Y. B. Shim, *Anal. Chem.*, 2009, **81**, 6604.

[31] Y. Bai, F. Feng, L. Zhao, C. Wang, H. Wang, M. Tian, J. Qin, Y. Duan, X. He, *Biosens. Bioelectron.*, 2013, **47**, 265.

[32] J. Zhao, F. Lin, Y. Yi, Y. Huang, H. Li, Y. Zhang and S. Yao, *Analyst*, 2012, **137**, 3488.

[33] A. Zheng, J. Wang, J. Li, X. Song, G. Chen, H. Yang, *Chem. Commun.*, 2012, **48**, 374.

[34] G. Z. Sauerbrey, *Z. Phys. A: Hadrons Nuclei*, 1959, **155**, 206.